Available online at www.sciencedirect.com
SCIENCE DIRECT®
Journal of Chromatography A, 1011 (2003) 111–123
JOURNAL OF CHROMATOGRAPHY A
www.elsevier.com/locate/chroma

Development of asymmetrical flow field-flow fractionation–multi angle laser light scattering analysis for molecular mass characterization of cationic potato amylopectin

Seungho Lee[a,1], Per-Ola Nilsson[b], Gunilla S. Nilsson[b], Karl-Gustav Wahlund[a,*]

[a]*Division of Technical Analytical Chemistry, Center for Chemistry and Chemical Engineering, Lund University, P.O. Box 124, S-221 00 Lund, Sweden*

[b]*Lyckeby Stärkelsen Research and Technology, SE-291 91 Kristianstad, Sweden*

Received 24 February 2003; received in revised form 26 June 2003; accepted 27 June 2003

Abstract

The goal of this study is to investigate the applicability of asymmetrical flow field-flow fractionation (AsFlFFF)–multi angle laser light scattering (MALLS), and to develop a method for analysis of cationic potato amylopectin (CPAP) having ultrahigh molecular mass (UHM_r). Use of the aqueous carrier having low salt content (3 m*M* NaN_3) resulted in a distortion in AsFlFFF fractograms of CPAP with a general pattern of a sharp rise at the beginning of the elution followed by a long tailing, probably due to combination of attractive and repulsive charge interactions (attractive interaction between CPAP molecules and the channel membrane, and repulsion among cationic CPAP molecules). As the cross flow-rate (F_c) increases, the tailing tends to increase, and the repeatability of the AsFlFFF retention data tends to decrease, which is an indication of the presence of the charge interactions. The tailing gradually decreased, and the repeatability of the AsFlFFF retention data increased, as the salt content of the carrier increased. The distortion of the fractogram finally disappeared at F_c of about 0.2 ml/min and the channel flow-rate (F_{out}) of about 1 ml/min with the aqueous carrier having the salt content of 40 m*M* (3 m*M* NaN_3+37 m*M* $NaNO_3$). The weight-average molecular mass (M_w) and the *z*-average radius of gyration ($\langle r_g \rangle_z$) determined by MALLS were 5.2×10^7 and 34×10^1 nm, respectively. With the flow-rate ratio, F_c/F_{out} kept constant, the degree of the charge interactions (and thus the distortion of fractogram) seems to increase with the cross flow-rate (F_c) and with the sample injection mass. AsFlFFF–MALLS was applied for determination of molecular mass distributions (M_rDs) and the sizes of CPAPs prepared by various cooking procedures.

Keywords: Asymmetrical flow field-flow fractionation; Multi-angle laser light scattering; Molecular weight distribution; Field-flow fractionation; Cationic potato amylopectin; Starch

1. Introduction

Starches are widely used in various industries, and are often modified (or derivatized) in order to expand their applicability and to obtain desired properties for particular applications [1]. To optimize the modi-

*Corresponding author. Tel.: +46-46-222-8316; fax: +46-46-222-4525.
E-mail address: karl-gustav.wahlund@teknlk.lth.se (K.-G. Wahlund).
[1]Present address: Department of Chemistry, Hannam University, Taejon 306-791, South Korea.

0021-9673/03/$ – see front matter © 2003 Published by Elsevier B.V.
doi:10.1016/S0021-9673(03)01144-0

fication and the processing (and thus the use) of starch materials, the knowledge of the relationship between the modification or the processing parameters and the properties of the final starch product is required, and thus the chemical and physical properties of the starch materials need to be measured. One of the most important properties of the starch materials is the molecular mass distribution (M_rD), as it affects the chemical, physical and rheological properties of the starch material.

Flow field-flow fractionation (FlFFF) is a technique that could be useful for analysis of ultra-large polymer molecules such as the starch materials. FlFFF provides separation of polymers based on the hydrodynamic size (or molecular mass, M_r), and some physical properties of the samples can be directly determined from their retention data. Applicability of FlFFF has been shown for analysis of various polymers and colloidal particles, including water-soluble polymers [2–7], humic acids [8], biological polymers [9], liposomes [10], DNAs [11], pigment particles [12], colloidal particles [13,14], ribosome [15], natural organic matters [16,17], wheat proteins [18], aquatic humic colloids [19].

In FlFFF, the diffusion coefficient (and thus the hydrodynamic diameter, d_H) of the sample can be directly determined from its retention data. In an asymmetrical flow field-flow fractionation (AsFlFFF), the relationship between d_H and the retention time, t_R is given by [15,20]:

$$d_H = \frac{2kTV^0}{\pi\eta F_c w^2 t^0} \cdot t_R \quad (1)$$

where k is the Boltzmann constant, T the absolute temperature (K), V^0 the channel void volume, η the viscosity, F_c the cross flow-rate, w the channel thickness, and t^0 the channel void time. Eq. (1) is a simplified expression that is applicable only to the cases of relatively high retention. With all experimental parameters fixed constant, d_H is directly proportional to t_R.

The application of Eq. (1) is limited to an ‘‘ideal’’ case where there are no charge interactions such as the interaction among the sample molecules or the interaction between the sample and the channel wall. An ideal condition must be provided in AsFlFFF analysis to obtain accurate results using Eq. (1).

There have already been a few studies on the retention behaviour of positively charged polymers in FlFFF [4,9] but these have been of low to high molecular mass. In this study the aim is to apply FlFFF to polymers of ultra-high molecular mass (UHM_r), i.e., $>10^7$. FFF analysis of ionic (or charged) species is challenging as it can be complicated by various forms of charge interactions during elution. The charge interactions will result in distortion in the elution profile and inaccurate retention data. The degree of charge interaction may vary with various parameters including the chemical and physical properties of the sample, the type and pH of the carrier, the type and the concentration of salts added in the carrier, and also with the type of the membrane (accumulation wall), etc. It has been shown that the retention of charged molecules or particles is sensitive to the type and the concentration of salts in the carrier, and generally an addition of a certain amount of salt into the carrier (thus increasing the ionic strength) suppresses the charge interactions of charged molecules or particles [7,13,21,22].

Multi angle laser light scattering (MALLS) is a technique that is useful for determination of bulk properties of polymeric samples, such as the average values of the M_r and the radius of gyration (r_g) [23]. The on-line coupling of MALLS with FlFFF (FlFFF–MALLS) becomes a powerful tool for determination of the distributions of the M_r and r_g. FlFFF provides size (or M_r)-based separation, and MALLS provides the M_r and r_g of each slice of the FlFFF fractogram, thus yielding distributions of M_r and r_g of the sample. FlFFF–MALLS has been used for analysis of various samples, including colloidal particles [14], water-soluble polymers [7], polysaccharides [24], celluloses [25], Dextran and tobacco mosaic virus [26], natural colloids [27], κ-carrageenan [28], polyacrylamide [29,30], κ-carrageenan and xanthan [31], and amylopectin [32].

Starch is comprised of two major components, amylopectin and amylose. The goal of this study is to investigate the applicability of AsFlFFF–MALLS for determination of M_rD and r_g of cationic potato amylopectin (CPAP), and also to compare CPAPs processed by various cooking procedures.

2. Experimental

2.1. Asymmetrical flow field-flow fractionation

The AsFlFFF channel was set up as described in previous studies [32,33] with a 130-μm-thick polyester spacer and a regenerated cellulose membrane (UF-C10, Hoechst) having an M_r-cutoff of 10,000. The channel geometry was trapezoidal [34,35] with the tip-to-tip length of 28.5 cm and the breadths at the inlet and the outlet of 2.0 and 0.5 cm, respectively.

The carrier was pure water containing various amounts of salt (NaN_3 and $NaNO_3$). For all AsFlFFF experiments, the sample was introduced into the channel using a 20-μl loop injector (Rheodyne, Cotati, CA, USA) by the following procedure. First the inlet flow-rate (F_{in}) was set at 1 ml/min, and the channel flow-outlet was closed. Now all the flow entering the channel exits through the cross flow-outlet. Then the valve on the cross flow-outlet tubing was opened to the atmosphere bypassing the needle valve. This reduces the channel pressure down to about 2~3 bar during the sample introduction and relaxation/focusing period. The sample was introduced by a syringe pump at 0.2 ml/min for 30 s. After the syringe pump was turned off, the sample was allowed to relax and focused for 30 s. After the relaxation and focusing, the inlet flow-rate was adjusted to the desired level and the valve on the cross flow-outlet tubing was returned to its normal elution position, at which point the data collection was started. During elution of the sample, the channel pressure reaches around 6~10 bar, depending upon the flow-rate conditions.

All samples were diluted with the carrier before the injection. Two on-line detectors were used, which were a DAWN-DSP MALLS detector (Wyatt Technology, Santa Barbara, CA, USA) followed by an Optilab DSP interferometric refractive index (RI) detector (Wyatt Technology). Both detectors were equipped with 633 nm lasers. A filter [Millipore Type RA 1.2 μm filter put into a high-performance liquid chromatography (HPLC) pre-column filter holder after being cut out by a hole puncher] was placed between the outlet of the channel and the MALLS detector to reduce the noise in light scattering data.

2.2. Cationic potato amylopectin

A CPAP sample (called ''CPAP'') was prepared as a test material for the applicability of AsFlFFF for CPAP analysis. It was 100% potato amylopectin (PAP) cationized by the reaction of PAP with 2,3-epoxy propyl trimethyl ammonium chloride. The degree of substitution (DS) was measured to be 0.061. This means that on average there were 6.1 substituents per 100 anhydroglucose units. The DS was calculated as $DS=(162N)/(14-151N)$, where N is the mass fraction of nitrogen in the sample, and 162, 151, and 14 are the molecular masses of the anhydroglucose unit, the substituent, and nitrogen, respectively. The samples were carefully washed with 50% ethanol before nitrogen determination according to the Kjeldahl method. A method was developed for dissolution of CPAP in water. First, CPAP was jet-cooked at 120 °C with a flow of 80 l/h without backpressure. No granules were found in the stock solution by optical microscopy. The viscosity of a 1% (w/v) jet-cooked solution of CPAP was approximately 100–200 cP at 50 °C. All other percentage concentrations in this work are also in w/v. The jet-cooked CPAP solution was freeze–dried. A 0.2% stock solution of CPAP was prepared by dissolving the freeze–dried CPAP in water containing 3 mM NaN_3 (0.02%) at 100 °C for 30 min in a Reacti-Therm (Pierce, Rockford, IL, USA) with constant stirring. The stock solution was diluted with carrier at 0.01~0.02% for AsFlFFF analysis. Previously measured dn/dc values for various starch derivatives were in the range between 0.145 and 0.155 ml/g, and a dn/dc value of 0.15 was used for light scattering calculations for all CPAP materials used in this study.

To study the effect of cooking conditions on the MWD of CPAP, two more samples of the CPAP (called ''CPAP≠1'' and ''CPAP≠2'', respectively) were prepared. Each of them was cooked by three different procedures, namely jet-cooking at 130 °C, jet-cooking at 140 °C, and batch-cooking at 95 °C, yielding three samples for each of CPAP≠1 and CPAP≠2 (six samples in total). For jet-cooking, 187 g of CPAP was slurried into 10 kg of deionized water, and then cooked in a heated continuous cooker (''jet-cooker'') at the flow-rate of about

80 l/h. During cooking, the pressures in the cooking zone were 2.4 and 1.7 bar, at the cooking temperatures of 140 and 130 °C, respectively. The viscosities, measured as 1% dry substance by a Brookfield viscometer (spindle 3, 100 rpm, 50 °C), were 111 and 160 cP for the CPAP≠1 cooked at 140 and 130 °C, respectively, and 105 and 122 cP for CPAP≠2 cooked at 140 and 130 °C, respectively. For batch-cooking, 5.5 g of dry CPAP was weighed in a 1000-ml glass beaker, and then deionized water was added to a total of 550 g. The beaker was placed in a boiling water bath (95 °C) for 30 min. During the batch-cooking, the slurry was stirred at 1000 rpm using a high shear stirrer. The viscosity of the batch-cooked CPAP, measured in the same way as above, was 437 cP, which is much higher than those of jet-cooked CPAPs. All preparations were freeze–dried and stock solutions prepared by dissolution as described above.

3. Results and discussion

3.1. Retention behaviour, ionic strength

Fig. 1 shows AsFlFFF elution profiles of CPAP obtained with water containing 3 m*M* (about 0.02%) NaN_3 as the carrier. The sample injection mass was 2.04 μg (20 μl injection of 0.0102% sample solution). The ratio of the cross flow-rate (F_c) to the channel flow-rate (F_{out}), F_c/F_{out} was varied while F_{in} was kept constant at 1.25 ml/min. The void times (t^0) were calculated by the AsFlFFF theory [34,36]. All fractograms in Fig. 1 show distorted elution profiles with a general pattern of a sharp rise at the beginning, followed by a long tail. The distortion becomes increasingly serious as F_c increases. At F_c of 0.91 ml/min, the tailing was so serious that the elution did not end until the run was terminated at 30 min.

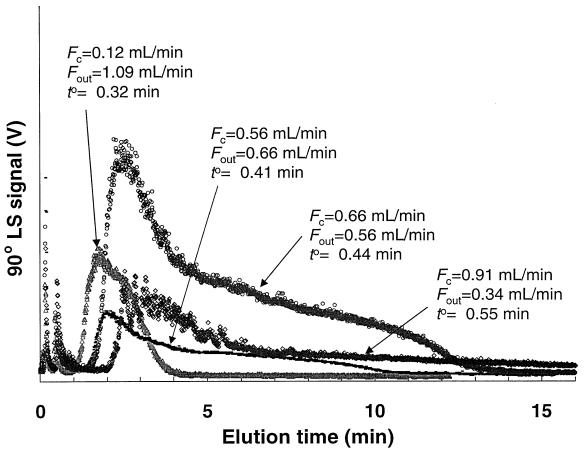

Fig. 1. AsFlFFF fractograms of CPAP obtained in water with 3 m*M* NaN_3. F_c/F_{out} was varied with F_{in} kept constant at about 1.2 ml/min. The sample injection mass was 2.04 μg (20 μl injection of 0.0102% solution).

In an ideal situation where charge interactions are absent, the ratio, t_R/t^0 is given by [20]:

$$\frac{t_R}{t^0} = \frac{w^2}{6DV^0} \cdot F_c \qquad (2)$$

With all other experimental parameters kept constant, the ratio t_R/t^0 of a sample is proportional to the cross flow-rate, F_c.

In Eq. (2), D is the diffusion coefficient of the sample. For many polymers, the diffusion coefficient is inversely dependent on the M_r [37]. With all the experimental parameters kept constant, AsFlFFF provides a separation based on the diffusion coefficient, and thus a separation based on the M_r. The retention time increases as D decreases or the M_r increases.

The ratio, t_R/t^0 and d_H calculated for the data shown in Fig. 1 are summarized in Table 1. For each fractogram, t_R was measured at three different positions (the maximum of the early eluting peak, the end of the tailing, and the midpoint between the previous two positions). For the fractogram obtained at $F_c = 0.91$, only one position was measured at the peak maximum as the end point of the elution was not clear due to tailing.

According to Eq. (2), the ratio, t_R/t^0 is expected to increase proportionally with F_c in an ideal condition. And, of course, the hydrodynamic diameter, d_H should remain constant even if the flow-rate changes. In Table 1, t_R/t^0 does not show a proportional increase with F_c. The t_R/t^0 measured at the peak maximum was even decreased (by 14%) when F_c was increased from 0.12 to 0.56 ml/min. The d_H values measured at all three positions of the fractogram were also decreased when F_c was increased

Table 1
AsFlFFF retention of CPAP in water with 3 m*M* NaN_3

F_c (ml/min)	F_{out} (ml/min)	F_c/F_{out}	t^0 (min)	Measured position	t_R (min)	t_R/t^0	d_H^* (nm)
0.12	1.09	0.11	0.32	Peak max	1.80	5.6	238 (21.2)
				Middle	3.10	9.7	416
				End	4.40	13.8	595
0.56	0.66	0.85	0.41	Peak max	1.96	4.8	43 (2.7)
				Middle	6.30	15.4	142
				End	10.5	25.6	239
0.66	0.56	1.18	0.44	Peak max	2.52	5.7	43 (5.2)
				Middle	8.00	18.2	142
				End	13.5	30.7	240
0.91	0.34	2.68	0.55	Peak max	3.44	6.3	35 (5.0)

The sample injection mass was 2.04 μg (20 μl injection of 0.0102% solution).
Numbers in parentheses are standard deviations. * Calculated by Eq. (1).

from 0.12 to 0.56 ml/min, indicating the sample elutes earlier than they should at higher F_c. At F_c higher than 0.56, t_R/t^0 increases with F_c as theory predicts (although it is not exactly proportional), and d_H tends to stay nearly constant.

The disagreement with theory discussed above in AsFlFFF retention behaviours of CPAP is probably due to the electrostatic repulsion between the cationic CPAP molecules. As F_c increases, molecules are pushed closer to the accumulation wall (forming a thinner layer close to the accumulation wall) and move closer to each other. The cationic molecules will then tend to repel each other and move away from the accumulation wall, and will be eluted earlier than they would in the absence of the charge interactions. As F_c increases further, molecules are pushed even closer to the membrane, and it seems that attractive interactions starts to come into play, causing long tailing as seen in Fig. 1 for F_c of 0.91 ml/min.

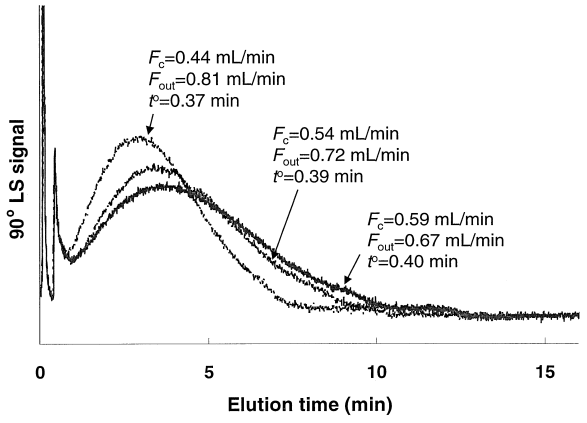

Fig. 2. AsFlFFF fractograms of CPAP obtained using an aqueous carrier with the total salt content of 20 m*M* (3 m*M* NaN_3 + 17 m*M* $NaNO_3$). F_c/F_{out} was varied while F_{in} was kept constant at about 1.2 ml/min. The sample injection mass was 4.08 μg (20 μl injection of 0.0204% solution).

Generally the charge interaction decreases in a medium with higher ionic strengths [13]. Fig. 2 shows AsFlFFF fractograms of CPAP obtained at various flow-rate combinations (F_c/F_{out}) using water with the total salt content of 20 m*M* (3 m*M* NaN_3 + 17 m*M* $NaNO_3$) as the carrier. The tailing still exists, but overall elution profiles of the fractograms were much improved compared to those in Fig. 1 (where the salt content of the carrier was 3 m*M*), probably due to reduced charge interactions.

The ratio, t_R/t^0 and d_H calculated at the peak maximum of the fractograms shown in Fig. 2 are summarized in the first three rows of Table 2. Overall, the t_R/t^0 values (and thus the d_H values) are higher than those measured at the peak maximum of the fractograms shown in Fig. 1 (see Table 1), and this increase in retention is probably due to reduced charge repulsion. As in Table 1, t_R/t^0 does not show

Table 2
AsFlFFF retention of CPAP in water with the total salt content of 20 m*M* (3 m*M* NaN_3 + 17 m*M* $NaNO_3$)

F_c (ml/min)	F_{out} (ml/min)	F_c/F_{out}	t^0 (min)	t_R (min)	t_R/t^0	d_H^* (nm)
0.44	0.81	0.54	0.37	3.19	8.6	101 (12.7)
0.54	0.72	0.75	0.39	3.48	8.9	85 (9.6)
0.59	0.67	0.88	0.40	4.36	10.9	95 (12.2)
1.16	1.36	0.85	0.20	2.86	14.3	64 (10.2)

The sample injection mass was 2.04 μg (20 μl injection of 0.0102% solution).
Numbers in parentheses are standard deviations. * Calculated by Eq. (1).

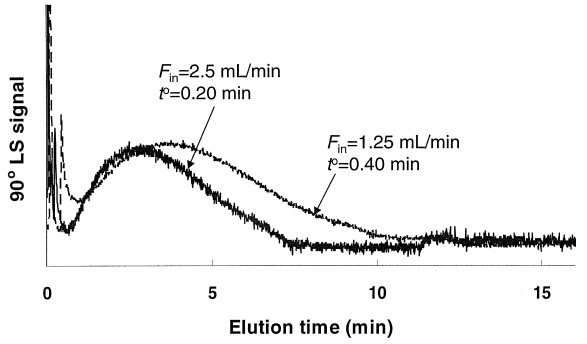

Fig. 3. AsFlFFF fractograms of CPAP obtained using an aqueous carrier with the total salt content of 20 m*M* (3 m*M* NaN_3 + 17 m*M* $NaNO_3$) at two different inlet flow-rates. F_c/F_{out} was kept constant at 0.86. The sample injection mass was 4.08 μg (20 μl injection of 0.0204% solution).

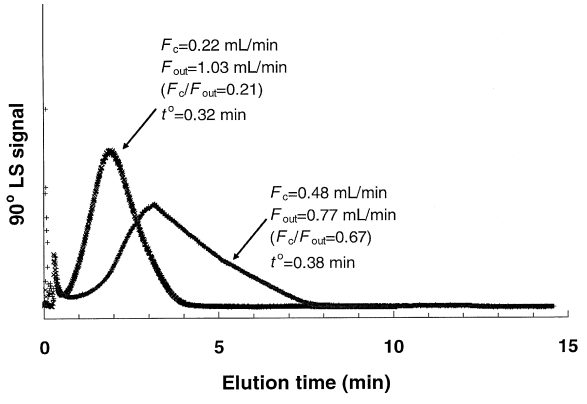

Fig. 4. AsFlFFF fractograms of CPAP obtained using an aqueous carrier with the total salt content of 40 m*M* (3 m*M* NaN_3 + 37 m*M* $NaNO_3$). F_c/F_{out} was varied while F_{in} was kept constant at 1.25 ml/min. For both runs, the sample injection mass was 4.08 μg (20 μl injection of 0.0204% solution).

the proportional increase with F_c, which suggests that there still exist charge interactions.

Fig. 3 shows two AsFlFFF fractograms of CPAP obtained using the same carrier as in Fig. 2 at two different inlet flow-rates (F_{in}) while keeping F_c/F_{out} constant at 0.86. The t_R/t^0 and d_H values calculated at the peak maximum of the fractograms shown in Fig. 3 are listed in the last two rows of Table 2. According to AsFlFFF theory, t_R should not change with F_{in} as long as the flow-rate ratio, F_c/F_{out}, is kept constant [36]. However, as shown in Fig. 3 and in the last two rows of Table 2, t_R was decreased from 4.36 to 2.86 min when F_{in} was increased from 1.26 to 2.52 ml/min, which may be another indication of non-ideality due to the charge interactions.

The total salt content was further increased to 40 m*M* (3 m*M* NaN_3 + 37 m*M* $NaNO_3$). Fig. 4 shows AsFlFFF fractograms of CPAP obtained at two different flow-rate conditions (F_c/F_{out} = 0.21 and 0.62) while F_{in} was kept constant at 1.25 ml/min. The fractogram obtained at F_c = 0.22 is almost of a Gaussian profile. However, at higher cross flow-rate (F_c = 0.50 ml/min, F_c/F_{out} = 0.67), the fractogram became distorted. This trend of increasing distortion of AsFlFFF fractogram with increasing F_c was reproducible.

The results shown in Fig. 4 are consistent with the results shown in Fig. 1 in that the distortion in the fractogram increases as the cross flow-rate, F_c, increases. This trend suggests that F_c needs to be kept as low as possible to reduce possible charge interactions when analyzing charged molecules using AsFlFFF. However F_c cannot be lowered too much as the retention (and thus the resolution) is then also lowered [11].

Table 3
AsFlFFF data of CPAP in water with the total salt content of 40 m*M* (3 m*M* NaN_3 + 37 m*M* $NaNO_3$)

F_c (ml/min)	F_{out} (ml/min)	F_c/F_{out}	t^0 (min)	t_R (min)	t_R/t^0	d_H^* (nm)
0.21	1.04	0.20	0.32	1.91	6.0	143
0.22	1.03	0.21	0.32	1.92	6.0	136
Av. 0.22	1.04	0.21	0.32	1.92 (0.01)	6.0	140 (5.0)
0.48	0.77	0.62	0.38	3.16	8.3	89
0.51	0.73	0.70	0.39	3.42	8.3	88
Av. 0.50	0.75	1.32	0.39	3.29 (0.18)	8.3	89 (0.71)

The injected sample mass was 4.08 μg (20 μl injection of 0.0204% sample solution).
Numbers in parentheses are standard deviations. * Calculated by Eq. (1).

The ratio, t_R/t^0 and d_H calculated for the peak maximum of the fractograms shown in Fig. 4 are summarized in Table 3. Each run was repeated twice, and all the results are shown with the averages. As mentioned earlier with Eq. (2), t_R/t^0 is proportional to F_c under ideal conditions. In Table 3, a 2.2-times increase in F_c (from 0.22 to 0.48 ml/min) resulted in only a 1.4-times increase in t_R/t^0 (from 6.0 to 8.3). And the measured d_H was even decreased from 136 to 89 nm. The decrease in measured d_H at higher F_c indicates that the sample was eluted earlier than it should at higher F_c, probably due to increased charge-repulsion. This result also suggests that F_c of 0.48 ml/min is too high for an ideal FFF behaviour of the CPAP used in this study. This increase in charge-repulsion may also be a cause for the distortion of the fractogram at F_c of 0.48 ml/min as shown in Fig. 4.

Based on the results obtained so far, F_c of 0.2~0.4 ml/min, F_{out} of 0.8~1 ml/min and the salt content of 40 m*M* were chosen for AsFlFFF–MALLS analysis of CPAP. At F_{out} of about 1 ml/min, F_c of higher than about 0.4 ml/min resulted in too high retention of the sample, causing tailing due to electrostatic interactions. At the same F_{out}, F_c of lower than about 0.2 ml/min resulted in too early elution of the sample.

3.2. Molecular mass distributions

As mentioned earlier, the multi angle light scattering detector, in combination with a concentration detector such as a RI detector, provides the weight-average molecular mass (M_w) and the *z*-average radius of gyration [or the root-mean-square (RMS) radius], $\langle r_g \rangle_z$, without the need for a system calibration [23]. In the light scattering detector used in this study, the scattered light intensity is measured at 15 different angles for each slice of the fractograms. In order to obtain M_w and $\langle r_g \rangle_z$, the light scattering signals are plotted against the angle (''Debye plot'') for the polynomial curve fitting. The curve fitting must be performed as accurate as possible as M_w and $\langle r_g \rangle_z$ are determined from the intercept and the slope of the polynomial curve at the zero angle, respectively.

There are a few parameters that need to be properly chosen for accurate curve fitting; the order of the polynomial function and the angles to be included for curve fitting. As M_w and $\langle r_g \rangle_z$ are

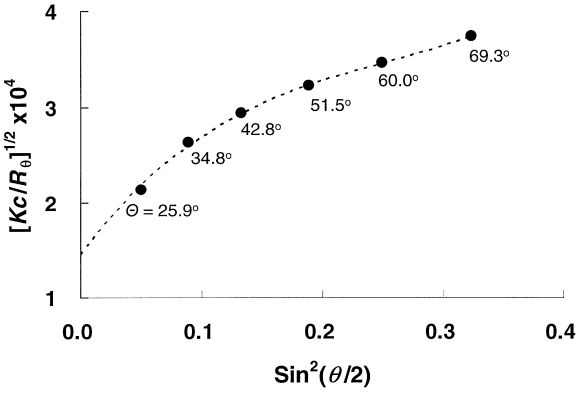

Fig. 5. Debye plot (presented by Berry method) of a slice at 1.93 min of the fractogram shown in Fig. 4 at F_c = 0.22 ml/min. Circles are the light scattering data and the dotted line is the result of a third-order polynomial fit.

determined from the intercept and the initial slope of the curve, the higher range of angles may not be needed as long as there are enough many angles in the low range available for extrapolation to zero angle. There are also three different ways of presenting the Debye plot. They are the Debye [23], the Zimm [38], and the Berry method [39]. For low-M_r polymers having $\langle r_g \rangle_z$ smaller than about 100 nm, the curve fitting is rather simple as the Debye plot is usually linear. However for high-M_r polymers, the Debye plot tends to deviate from the linearity and requires careful examination for accurate curve fitting.

For the fractograms shown in Fig. 4, the Berry method with a third-order polynomial fitting yielded the best results. Fig. 5 shows a Debye plot presented by the Berry method for the slice at the retention time of 1.93 min of the fractogram obtained at $F_c = 0.22$ ml/min. The circles are the light scattering data measured by MALLS at the six different angles of 25.9, 34.8, 42.8, 51.5, 60.0, and 69.3°, respectively, and the dotted line is the result of a third-order polynomial fitting for the six data points. Although there are 15 angles available in total, only the mentioned six were needed for the curve fitting. Moreover, the use of higher angles resulted in rather large imprecision in both M_w and $\langle r_g \rangle_z$ data. The M_w and $\langle r_g \rangle_z$ for this slice are $4.8 \cdot 10^7$ g/mol and $32 \cdot 10^1$ nm, respectively. Fig. 6 shows the fractograms shown in Fig. 4 overlaid with the M_w determined by MALLS for each slice. In both cases, the M_r increases with time, showing the capability of AsFlFFF for M_r-based separation, as mentioned earlier with Eq. (2). It is noteworthy that the size-resolution was somewhat improved by using higher cross flow-rate ($F_c = 0.48$ ml/min), enabling detection of both lower and higher ends of the distribution than at lower cross flow-rate ($F_c = 0.22$ ml/min). This is caused by the higher level of retention obtained by higher cross flow-rate as explained with Eq. (2).

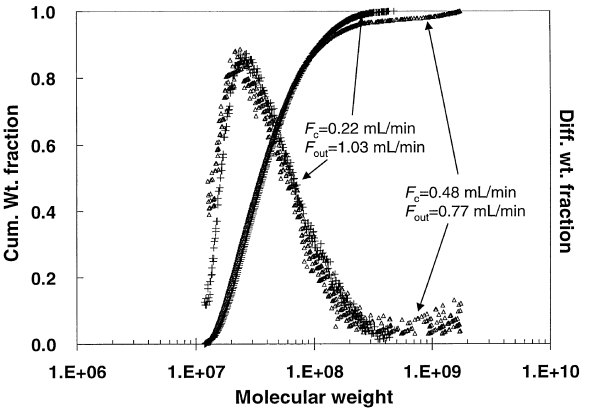

Fig. 7. Differential and cumulative molecular mass distributions of CPAP obtained for the fractograms shown in Fig. 4.

Figs. 7 and 8 show M_rDs and the size distributions obtained by MALLS for the fractograms shown in Fig. 4. In Fig. 7, the two M_rDs are similar, as they should be, despite the difference in FFF retention

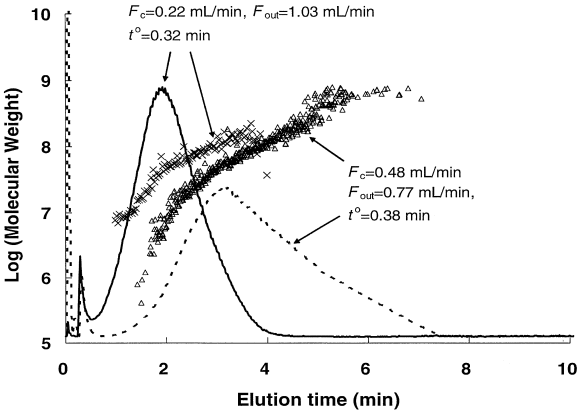

Fig. 6. AsFlFFF fractograms (shown in Fig. 4) and molecular masses of CPAP determined by MALLS.

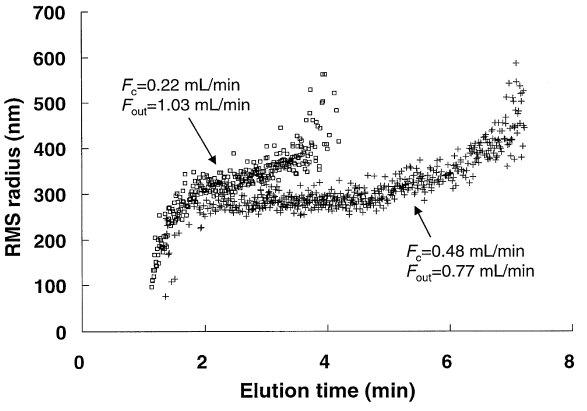

Fig. 8. RMS radius distributions obtained for the fractograms shown in Fig. 4.

behaviour (see Table 3) and the distorted peak profile obtained at $F_c = 0.48$ ml/min. Here, the improved resolution at the high-M_r end when using the higher crossflow-rate is clearly visible. It is interesting, that even if the elution profile was distorted, the system still separates by molecular mass. In Fig. 8, the size gradually increases with time in both cases, as expected.

The M_w and $\langle r_g \rangle_z$ obtained for the two fractograms shown in Fig. 4 are summarized in Table 4. Despite of the differences in FFF retention data (see Table 3) between two fractograms, both the average molecular mass and the RMS radius are in agreement within one standard deviation. It is noted that, at F_c of 0.50 ml/min, the standard deviations in both M_w and $\langle r_g \rangle_z$ are higher than those at F_c of 0.22 ml/min. This higher standard deviation at higher F_c may be related with higher charge interaction, which needs further investigation. It needs to be mentioned here that accurate measurement of radii in this large size range is difficult as it is often subject to relatively large uncertainties and error. The sharp increases in size at the both ends of the plots shown in Fig. 8 may be the results of relatively large uncertainties caused by the low signal-to-noise ratio at the both ends of the RI and MALLS fractograms.

3.3. Sample concentration effects

Fig. 9 shows two AsFlFFF fractograms of CPAP obtained at the same condition ($F_c = 0.5$, $F_{out} = 0.75$), but with different sample concentrations (0.0204 and 0.0408%). The injection volume was the same at 20 μl, and thus the injected sample masses were 4.08 and 8.16 μg, respectively. As the sample concentration (thus the injection mass) increases, the molecules tend to be eluted earlier and the fractogram becomes more distorted, probably due to the increase in charge interactions. The FFF retention data measured for the peak maximum of the two fractograms shown in Fig. 9 are shown in Table 5. As expected, the measured d_H was decreased at higher sample concentration. In Fig. 9, both fractograms seem to come down to the baseline at around 7.8 min. The t_R/t^0 and d_H calculated for the elution time of 7.8 min were 20.5 and 220 nm, respectively. M_w and $\langle r_g \rangle_z$ determined by MALLS are shown in Table 6. As in Table 4, both M_w and $\langle r_g \rangle_z$ did not change significantly (within one standard deviation) with the sample concentration (injection mass), even if the AsFlFFF retention data (and thus d_H) were different (see Table 5). This proves the advantage of the independent M_r and r_g measurement by MALLS, the results of which are also evident by the rather similar molecular mass distributions shown in Fig. 10.

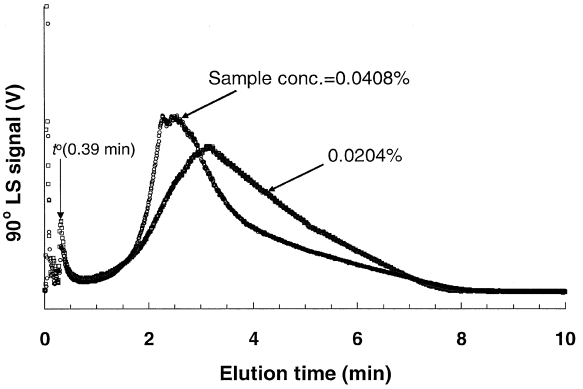

Fig. 9. AsFlFFF fractograms of CPAP obtained in an aqueous carrier with the total salt content of 40 m*M* (3 m*M* NaN_3 + 37 m*M* $NaNO_3$) at two different sample concentrations (0.0204 and 0.0408%). The injection volume was the same at 20 μl, thus the sample injection mass was 4.08 and 8.16 μg, respectively. F_c and F_{out} were 0.5 and 0.75 ml/min, respectively.

Table 4
Molecular mass and size of CPAP obtained from the light scattering data shown in Fig. 4

F_c (ml/min)	F_{out} (ml/min)	M_w	$\langle r_g \rangle_z$ (nm)
0.22	1.04	5.16 (0.44)·10^7	336 (2.1)
0.50	0.75	5.97 (1.64)·10^7	318 (20.6)

The sample injection mass was 4.08 μg (20 μl injection of 0.0204% sample solution).
Numbers in parentheses are standard deviations.

Table 5
AsFlFFF retention of CPAP shown in Fig. 9

Sample concentration (%)	t^0 (min)	t_R (min)	t_R/t^0	d_H^* (nm)
0.0204	0.39	3.29	8.3	89 (0.71)
0.0408	0.39	2.52	6.6	69 (3.8)

$F_c = 0.5$, $F_{out} = 0.75$ ml/min, and the carrier was the same as that used in Fig. 4.
* Calculated by Eq. (1).

Table 6
Molecular mass and size of CPAP obtained for the fractograms shown in Fig. 9

Sample concentration (%)	Sample injection mass (μg)	M_w	$\langle r_g \rangle_z$ (nm)
0.0204	4.08	$5.97\ (1.64)\cdot 10^7$	318 (20.6)
0.0408	8.16	$6.66\ (1.69)\cdot 10^7$	265 (30.2)

$F_c = 0.5$, $F_{out} = 0.75$ ml/min, and the carrier was the same as that used in Fig. 4.
Numbers in parentheses are standard deviations.

3.4. Effects of cooking conditions

All six samples of CPAP#1 and #2 were analyzed by AsFlFFF/MALLS at two different flow-rate conditions (F_c/F_{out} of 0.2/1 and 0.38/0.84 ml/min). For the batch-cooked samples of CPAP#1 and 2, the channel flow-rate (F_{out}) decreased continuously quickly after the injection, and thus it was not possible to obtain meaningful fractograms. It seemed that the batch-cooked samples still contained starch granules that caused a blockage of the filter that is placed between the AsFlFFF channel and the MALLS. Figs. 11 and 12 show fractograms (RI signals) and M_r values of jet-cooked CPAPs obtained at F_c/F_{out} of 0.2/1 (Fig. 11) and 0.38/0.84 (Fig. 12), respectively. Again the resolution was improved when F_c was increased from 0.2 to 0.38 ml/min, and a broader range of M_r values was detected. For all

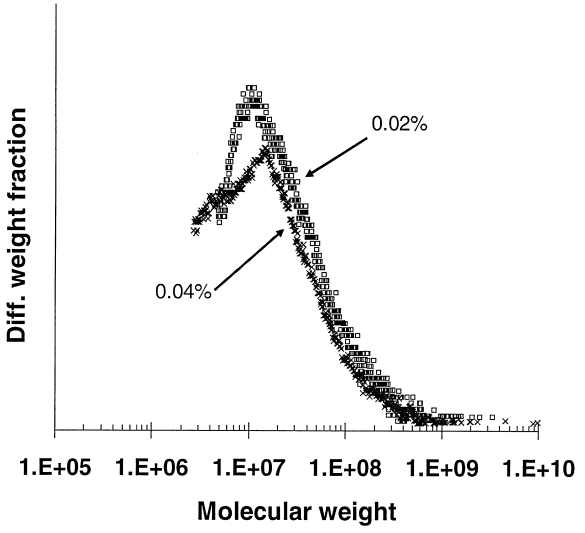

Fig. 10. Differential molecular mass distributions obtained by MALLS for the fractograms shown in Fig. 9.

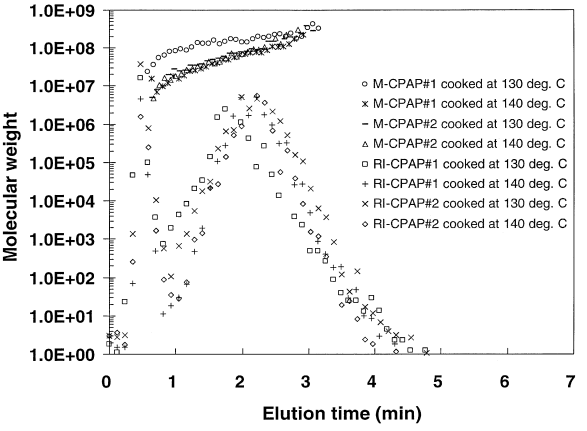

Fig. 11. AsFlFFF fractograms (RI signal) and molecular masses of jet-cooked CPAPs obtained in the same carrier as in Fig. 9 (40 mM salt content) at F_c of 0.2 and F_{out} of 1 ml/min. For better visibility only a fraction of the data points are shown.

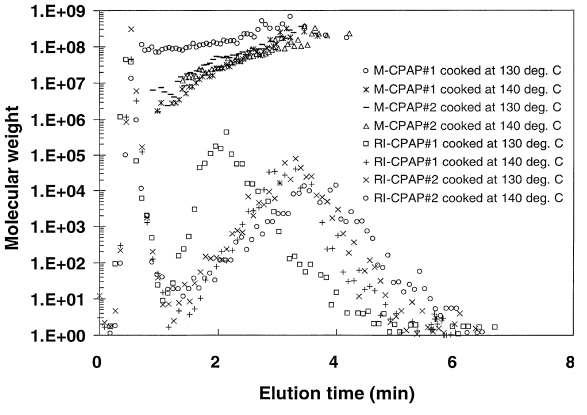

Fig. 12. AsFlFFF fractograms (RI signal) and molecular masses of jet-cooked CPAPs obtained in the same carrier as in Fig. 9 at F_c of 0.38 and F_{out} of 0.84 ml/min. For better visibility only a fraction of the data points are shown.

samples, the M_r increases as the elution time increases, showing the separation by AsFlFFF based on the M_r.

In both Figs. 11 and 12, the M_r data of the CPAP≠1 jet-cooked at 130 °C are different from those of the others. It spans a higher, but narrower range of M_r. This deviation may be related with the fact that the CPAP≠1 jet-cooked at 130 °C had significantly higher viscosity than the other three samples (see Experimental section) which suggests that it had been much less degraded by the jet-cooking procedure. It should be mentioned that it can be difficult to fine-tune the conditions in a jet cooker to reach high reproducibility and this can explain the deviating result. Moreover, for the same elution time, the CPAP≠1 jet-cooked at 130 °C has a higher M_r than the others. This may suggest the CPAP≠1 jet-cooked at 130 °C has a different molecular conformation than the others so that the hydrodynamic diameter, d_H, may have a different relationship to the molecular mass, i.e., a more dense structure. More likely however, there is an error in the hydrodynamic diameter, as calculated from the retention time through Eq. (1), which is caused by too early elution. This is clearly noted in Fig. 12 where the CPAP≠1 jet-cooked at 130 °C is eluted much earlier than the others despite of its higher M_r. This is not the expected behaviour in the normal mode of flow FFF, where the retention time increases with d_H (or M_r) as shown in Eq. (1).

The erroneous d_H is obvious in Table 7 where use of the higher $F_c = 0.38$ ml/min results in about half the observed d_H as compared to at $F_c = 0.2$ ml/min, unlike for the other samples. For the latter there is also a trend to lower observed d_H but much less pronounced and this can be explained by the influence of electrostatic repulsion as discussed above. The deviating behavior of the CPAP≠1 jet-cooked at 130 °C could be a result of a mixed mode retention mechanism where, due to the large size, the retention mode is partly that of the steric or lift-hyperlayer mode, which causes a reversal of the elution order in relation to the size. Such effects have been observed before for ultra-large macromolecules such as undegraded, underivatized potato amylopectin [32].

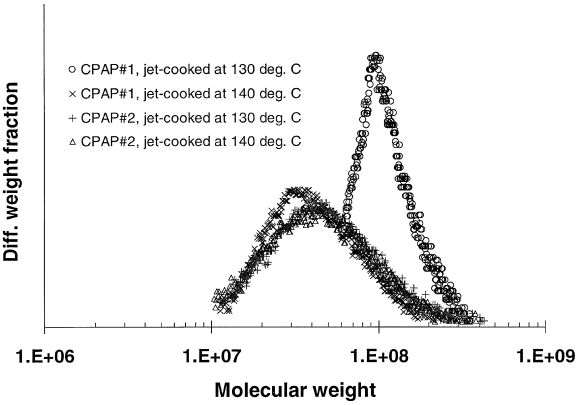

Fig. 13. Differential molecular mass distributions of jet-cooked CPAPs obtained under the same conditions as Fig. 11.

The deviating character of CPAP≠1 jet-cooked at 130 °C becomes even clearer in Figs. 13 and 14

Table 7
AsFlFFF/MALLS data of jet-cooked CPAPs in water with the total salt content of 40 m*M* (3 m*M* NaN_3 + 37 m*M* $NaNO_3$)

F_c (ml/min)	F_{out} (ml/min)	Sample	Cooking temperature (°C)	Injection mass (μg)	t^0 (min)	t_R (min)	t_R/t^0	d_H^* (nm)	M_w ($\cdot 10^6$)	$\langle r_g \rangle_z$ (nm)
0.2	1.0	CPAP≠1	130	7.3	0.34	1.42	4.2	111	120	337
			140	7.5	0.34	1.76	5.2	138	47	265
		CPAP≠2	130	8.3	0.33	1.73	5.2	130	63	231
			140	7.3	0.33	1.75	5.3	131	55	218
0.38	0.84	CPAP≠1	130	7.3	0.36	1.63	4.5	63	117	324
			140	7.5	0.36	2.65	7.4	103	39	231
		CPAP≠2	130	8.3	0.37	2.58	7.0	91	53	277
			140	7.3	0.37	3.07	8.3	103	49	274

* Calculated by Eq. (1).

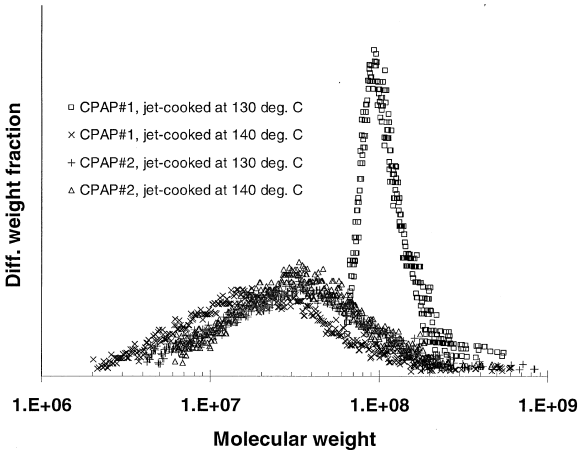

Fig. 14. Differential molecular mass distributions of jet-cooked CPAPs obtained under the same conditions as Fig. 12.

where the M_rDs are demonstrated based on the data shown in Fig. 11 (F_c/F_{out} of 0.2/1) and Fig. 12 (F_c/F_{out} of 0.38/0.84), respectively. In both Figs. 13 and 14, the CPAP≠1 jet-cooked at 130 °C has the highest M_r and the narrowest M_rD among all four samples. The M_rD became narrower at higher cross flow-rate as shown in Fig. 14, as opposed to those of the other samples. For the latter the wider M_rD reflects the improvement in size separation resolution obtained by the increased retention level caused by the increased cross flow-rate. The narrower observed apparent M_rD for the CPAP≠1 jet-cooked at 130 °C instead demonstrates a deteriorated size separation resolution which would be the result of the mixed-mode retention mechanism discussed above. Then the MALLS detector senses a mixture of different sizes in each measured slice instead of a narrow size range. Further investigation is needed for more detailed discussion on this matter.

All AsFlFFF/MALLS data are summarized in Table 7. At F_c/F_{out} of 0.2/1 and 0.38/0.84 ml/min, the CPAP≠1 jet-cooked at 140 °C has M_w values of $4.7\cdot10^7$ and $3.9\cdot10^7$, respectively, which are much lower than those of the same sample cooked at 130 °C ($1.2\cdot10^8$ and $1.2\cdot10^8$). This suggests the CPAP≠1 was significantly more degraded at 140 °C than at 130 °C. Also the CPAP≠1 jet-cooked at 140 °C has the lowest M_w among all four cooked samples, indicating it has been more degraded than the others.

Unlike the CPAP≠1, the CPAP≠2 jet-cooked at 130 and 140 °C do not show much difference in M_rD (see Figs. 13 and 14). At F_c/F_{out} of 0.2/1, with the cooking temperature lowered by 10 °C, M_w and $\langle r_g\rangle_z$ of the CPAP≠2 was reduced slightly from $6.3\cdot10^7$ and $23\cdot10^1$ nm down to $5.6\cdot10^7$ and $22\cdot10^1$ nm, respectively. At F_c/F_{out} of 0.38/0.84 ml/min, they were reduced from $5.4\cdot10^7$ and $28\cdot10^1$ nm down to $4.9\cdot10^7$ and $27\cdot10^1$ nm, respectively. This result indicates, for the CPAP≠2, that there is no significant difference in the degree of degradation during the jet-cooking at 130 and 140 °C.

4. Conclusion

The results of this study show the capability of AsFlFFF for M_r-based (or size-based) separation of charged polymers having ultrahigh molecular mass, such as CPAP. When analyzing charged polymers with AsFlFFF, an effort should be made to reach the ''ideal'' condition, where no charge interactions are present. This study shows one example of such an effort aimed at developing an AsFlFFF method for analysis of CPAP. Results obtained in this study suggest that F_c of 0.2~0.4 ml/min, F_{out} of 0.8~1 ml/min, and the salt content of 40 mM are appropriate for AsFlFFF–MALLS analysis of CPAP.

Different approaches may be required for different charged samples as the degree of charge interactions may vary with various chemical and physical properties of the sample (e.g., charge density and M_r), the composition and pH of the carrier, the type and the concentration of salts added in the carrier, and also the type of the channel membrane, etc. The behaviour in FlFFF of charged water-soluble polymers been studied previously [4,9,40]. A detailed discussion on the retention behaviour of polyvinylpyridin [40] regarding ionic strength and sample mass load largely confirms the findings for CPAP in the present study. However, polyvinylpyridin has a high charge density (unity charge per monomer residue) whereas CPAP has a much lower charge density (0.061 charges per monomer residue).

In addition to the salt content, the sample concentration (or the sample mass) is another factor that may require careful attention in optimization of

AsFlFFF for analysis of charged polymers. It is noted that the sample mass used in this study was lower than about 8 μg (20 μl injection of about 0.04% sample solution), which is much lower than that usually used in FlFFF experiments. Although it has not been thoroughly investigated in this study, it is believed that the use of low sample mass helps reducing the charge interactions among charged molecules.

It is evident that a study of the M_rD by AsFlFFF/MALLS can reveal variations in the effect on molecular degradation caused by the technological treatment of a starch derivative.

Acknowledgements

This work was financially supported by a grant from the Lyckeby Stärkelsen Research Foundation, from the Centre for Amphiphilic Polymers from Renewable Sources at Lund University, and from the Swedish Natural Science Research Council. This work was also supported by a Korea Research Foundation grant (KRF-2002-013-D00060).

References

[1] B. Raton, in: O.B. Wurzburg (Ed.), Modified Starches: Properties and Uses, CRC Press, Boca Raton, FL, 1987.
[2] J.C. Giddings, G.-C. Lin, M.N. Myers, J. Liq. Chromatogr. 1 (1978) 1.
[3] S.L. Brimhall, M.N. Myers, K.D. Caldwell, J.C. Giddings, J. Polym. Sci., Polym. Lett. Ed. 22 (1984) 339.
[4] M.A. Benincasa, J.C. Giddings, Anal. Chem. 64 (1992) 790.
[5] J.J. Kirkland, C.H. Dilks Jr., S.W. Rementer, Anal. Chem. 64 (1992) 1296.
[6] M.-A. Benincasa, K.D. Caldwell, J. Chromatogr. A 925 (2001) 159.
[7] H. Thielking, W.-M. Kulicke, Anal. Chem. 68 (1996) 1169.
[8] R. Beckett, Z. Jue, J.C. Giddings, Environ. Sci. Technol. 21 (1987) 289.
[9] J.C. Giddings, M.A. Benincasa, M.-K. Liu, P. Li, J. Liq. Chromatogr. 15 (1992) 1729.
[10] M.H. Moon, J.C. Giddings, J. Pharm. Biomed. Anal. 11 (1993) 911.
[11] M.-K. Liu, J.C. Giddings, Macromolecules 26 (1993) 3576.
[12] T. Schauer, Part. Part. Syst. Charact. 12 (1995) 284.
[13] M.H. Moon, Bull. Korean Chem. Soc. 16 (1995) 613.
[14] H. Thielking, D. Roessner, W.-M. Kulicke, Anal. Chem. 67 (1995) 3229.
[15] M. Nilsson, S. Birnbaum, K.-G. Wahlund, J. Biochem. Biophys. Methods 33 (1996) 9.
[16] G. Newcombe, M. Drikas, S. Assemi, R. Beckett, Water Res. 31 (1997) 965.
[17] C. Pelekani, G. Newcombe, V.L. Snoeyink, C. Hepplewhite, S. Assemi, R. Beckett, Environ. Sci. Technol. 33 (1999) 2807.
[18] S.G. Stevenson, T. Ueno, K.R. Preston, Anal. Chem. 71 (1999) 8.
[19] N.M. Thang, H. Geckeis, J.I. Kim, H.P. Beck, Colloids Surfaces A: Physicochem. Eng. Aspects 181 (2001) 289.
[20] B. Wittgren, K.-G. Wahlund, H. Derand, B. Wesslen, Macromolecules 29 (1996) 268.
[21] M.E. Hansen, J.C. Giddings, Anal. Chem. 61 (1989) 811.
[22] B. Wittgren, K.-G. Wahlund, H. Derand, B. Wesslen, Langmuir 12 (1996) 5999.
[23] P. Wyatt, Anal. Chim. Acta 272 (1993) 1.
[24] B. Wittgren, K.-G. Wahlund, J. Chromatogr. A 760 (1997) 205.
[25] B. Wittgren, K.-G. Wahlund, J. Chromatogr. A 791 (1997) 135.
[26] H. Thielking, W.-M. Kulicke, J. Microcol. Sep. 10 (1998) 51.
[27] F.v.d. Kammer, U. Forstner, Water Sci. Technol. 37 (1998) 173.
[28] B. Wittgren, J. Borgstrom, L. Piculell, K.-G. Wahlund, Biopolymers 45 (1998) 85.
[29] R. Hecker, P.D. Fawell, A. Jefferson, J.B. Farrow, J. Chromatogr. A 837 (1999) 139.
[30] R. Hecker, P.D. Fawell, A. Jefferson, J.B. Farrow, Sep. Sci. Technol. 35 (2000) 593.
[31] C. Viebke, P.A. Williams, Food Hydrocolloids 14 (2000) 265.
[32] M.v. Bruijnsvoort, K.-G. Wahlund, G. Nilsson, W.Th. Kok, J. Chromatogr. A 925 (2001) 171.
[33] K.-G. Wahlund, in: M.E. Schimpf, K.D. Caldwell, J.C. Giddings (Eds.), Field-Flow Fractionation Handbook, Wiley, New York, 2000, Chapter 18.
[34] A. Litzen, K.-G. Wahlund, Anal. Chem. 63 (1991) 1001.
[35] A. Litzen, Anal. Chem. 65 (1993) 461.
[36] K.-G. Wahlund, J.C. Giddings, Anal. Chem. 59 (1987) 1332.
[37] C. Tanford, in: Physical Chemistry of Macromolecules, Wiley, New York, 1961, Chapter 6.
[38] B.J. Zimm, J. Chem. Phys. 16 (1948) 1093.
[39] G.C. Berry, J. Chem. Phys. 44 (1966) 4550.
[40] M.A. Benincasa, J.C. Giddings, J. Microcol. Sep. 9 (1997) 479.